Appendix A.

CONTENTS: Narrative on "Materials and Methods" and "Discussion of Band Gap Data", 3 Data Tables, and 4 Figures.

A1. Materials and Methods.

A1.1 Nanoparticles and reagents

Transition metal oxide NPs (TiO_2, Cr_2O_3, Mn_2O_3, Fe_2O_3, NiO, CuO, and ZnO) were purchased from Nanostructured and Amorphous Materials (99.9% purity; Los Alamos, New Mexico, USA) and used as received. Immortalized human bronchial epithelial cells (BEAS-2B), human bronchoalveolar carcinoma-derived cells (A549), and fetal bovine serum were purchased from the American Type Culture Collection (ATCC) (Manassas, VA, USA). BEAS-2B basal culture medium and supplemental growth factors were purchased from Lonza (Basel, Switzerland). Ham's F-12 medium with L-glutamine was purchased from Fisher Scientific (Pittsburgh, PA, USA). Trypsin-EDTA and Hank's balanced salt solution (HBSS) were purchased from Invitrogen (Carlsbad, CA, USA). Sulforhodamine B (SRB) was purchased from ICN Biomedicals (Irvine, CA, USA). Ultrapure DI-water was prepared using a Milli-Q system (Millipore, Bedford, MA, USA). Reagents for inductively coupled plasma mass spectrometry (ICP-MS) and graphite furnace atomic absorption spectrophotometer (GFAA) were of the highest grade available (Fisher Scientific, Pittsburgh, PA, USA).

A1.2 Particle morphology, size, surface area, and isoelectric point determination

Particle morphology and size were characterized using transmission electron microscopy (TEM) with a JEOL 1400 instrument operated at 120 kV. Approximately 1 mg of each nanoparticle was placed in 1 mL of doubly distilled deionized water in an Eppendorf tube and sonicated. Microliter aliquots were applied to 400-mesh carbon-coated copper grids (Electron Microscopy Sciences) and allowed to dry in N_2 atmosphere

prior to microscopy. TEM images were saved in TIFF file format and examined using ImageJ ver. 1.44 software (National Institutes of Health, Gaithersburg, MD) to determine individual particle size and generate resulting histograms.

BET specific surface areas (SSA, m^2/g) of the nanoparticles were measured using a Quantachrome Autosorb 1-C instrument and N_2 as the probe molecule [1]. Samples were outgassed to expel moisture and weighed to determine dry mass of the nanoparticles. Seventy-eight data point complete gas adsorption isotherms were used to determine the specific surface areas.

Interactions of cellular material with metal oxide nanoparticles are primarily Coulombic in nature. Hence, electrostatic attractions need to be quantified with each respective metal oxide nanoparticle. IUPAC defines the potential difference with respect to the potential charge as:

$$E_{PZC} = E - E_{\sigma=0} \quad (1)$$

where E_{pzc} is the electrode potential difference with respect to point of zero charge, E is the potential of the same electrode against a defined reference electrode, and $E_{\sigma=0}$ is the potential of the same electrode with a zero surface charge. In practice, we measured the isoelectric point of each nanoparticle by monitoring the pH at the solid-aqueous solution interface using a spear-tip probe. Hence, the definition of the point-of-zero charge (PZC) used in our methodology is the pH value at which the solid surface is electrostatically neutral under aqueous solution conditions due to the absorption of equal amounts of hydronium and hydroxyl ions at the electrical double layer [2]. The PZC measurement method used was based on the original description by Park and Regalbuto [3], and modified for use to measure PZC of nanomaterials in our laboratory [4]. The procedure is

as follows: Solutions in the range of pH = 1.0–13.0 were prepared using dilute aqueous solutions of NaOH and HCl in doubly distilled, deionized Millipore water. A 1.8 mL aliquot of each solution was pipetted into polyethylene vials and allowed to equilibrate for 1 hr. The initial pH of the solution was measured and recorded. A 10.0 mg amount of each metal oxide nanoparticle powder was then added to the solution and allowed to settle to the bottom of the polyethylene tube. After an additional 16-hr equilibration period, the final pH of the nanoparticle surface was measured using a spear tip semisolid electrode. Plots of initial versus final pH values revealed plateaus denoting the PZC for each metal oxide.

A1.3 X-ray photoelectron spectroscopy (XPS)

The relative number of available particle surface binding sites was quantified using deconvoluted XPS integrated peak areas of the O 1s orbital of the nanoparticle surfaces, acquired using a Kratos Axis 25 XPS spectrometer. XPS is a non-destructive surface sensitive technique in which the kinetic energy of the analyte electrons is measured. The binding energy of the photoelectron is given by the relation:

$$BE = h\nu - (E_{kinetic} + \Phi) \quad (2)$$

where $h\nu$ is the energy of the X-ray photon, $E_{kinetic}$ is the kinetic energy of the electrons being measured, BE is the binding energy, and Φ is the work function of the instrument [5]. Spectral plots of counts of kinetic energy detected as a function of $E_{binding}$ were deconvoluted to quantify the amount of adsorbed and non-adsorbed (metal oxide) oxygen on the NP surface. In our experiments, the different oxidation states of the O 1s orbital peaks were deconvoluted to determine the contributions of metal oxide oxygen of the NP solid surface and non-metal oxide species adsorbed to the overall peak envelope. In all

spectral studies, the limiting case that all non-metal oxide oxidation states denoted adsorption to available sites on the NP surface was assumed.

For XPS analysis, NPs were collected from the CC reservoir by vacuum filtration using a Buchner funnel and a Fluoropore PTFE membrane filter paper with a 0.2 micron pore size (Billerica, MA). The NP solids were then mounted onto the XPS sample holder by cutting the membrane filter into 1 cm × 1 cm x 0.1mm squares and affixing the Teflon filter paper using Scotch 3M double-sided tape. Complete coverage of the membrane filter paper was denoted by the absence signal from the F 1s orbital in the XPS emanating from the underlying PTFE membrane. Charge correction was performed using the C 1s binding energy at 284.7 eV, denoting adventitious carbon from the atmosphere [6, 7]. XPS scans were obtained with a Mg Kα anode operated at 225 W and a photon energy of hν = 1253.6 eV and a base pressure that did not exceed 1.0 x 10^{-8} Torr. Physiosorbed oxygen and metal oxide, emanating from various chemical oxidation states, were deconvoluted using CasaXPS VAMAS processing software (Devon, United Kingdom) with Shirley background subtraction [8] and 70:30 Gaussian-Lorenztian lineshapes. Integrated peak area ratios of the physisorbed-to-metal oxide oxygen, obtained from curvefitting deconvoluted oxidation states from the XPS O 1s core level, were used as a means of quantifying the relative number of binding sites available to bind intracellular material on the metal oxide nanoparticulate surface. The non-metal oxide oxidation state(s) denote available binding sites emanating from those species adsorbed onto the NP surfaces. Under physiological conditions, these adsorbates would be from cellular material that could adsorb onto these same sites. Division by integrated peak areas of the metal oxide oxidation state was used to normalize for the relative number of binding sites, allowing

comparison of all fourth period metal oxide NPs. The procedure used normalize O 1s signals from the metal oxide in our laboratory is described elsewhere [9]. For example, an increased non-metal-oxide-to-metal oxide ratio denotes an increase in the number of surface binding sites on the nanoparticulate surface to cellular material.

A1.4 Quantification of available binding sites on NP surface

The constant composition (CC) procedure was conducted as follows: transition metal oxide nanoparticles were reacted in a 702 Titrino MetroOhm AG CH-9191 constant composition reactor (Herisau, Switzerland) adjusted to pH = 7.4 (±0.1) and maintained for a 24-h period. Using the autotitrator, HCl or NaOH was added dropwise to maintain constant pH. Since colloidal suspensions tended to approach pH values equal to that of the PZC along with absorption of adventitious atmospheric CO_2, HCl was almost exclusively added throughout the duration of the experiment. All solutions were prepared using doubly distilled, deionized Millipore water as the solvent. The CC reactor colloidal suspensions were prepared by adding 125 mg of the metal oxide to 25.0 mL of 0.01 M NaCl solution (with NaCl serving as background electrolyte) [9, 10] to stabilize pH. The solution was stirred during the CC reactions. During CC reactions, aliquots (4 mL each) of the solution were obtained at 3, 6, 9, 12, and 15 hr intervals, stored in glass tubes, and refrigerated at 5^{o}C for metal ion dissolution using ICP-MS and GFAA. Solid samples of metal oxide NPs from each 16-hr batch solution reaction) were extracted via vacuum filtration and saved for X-ray photoelectron spectroscopy (XPS) analysis.

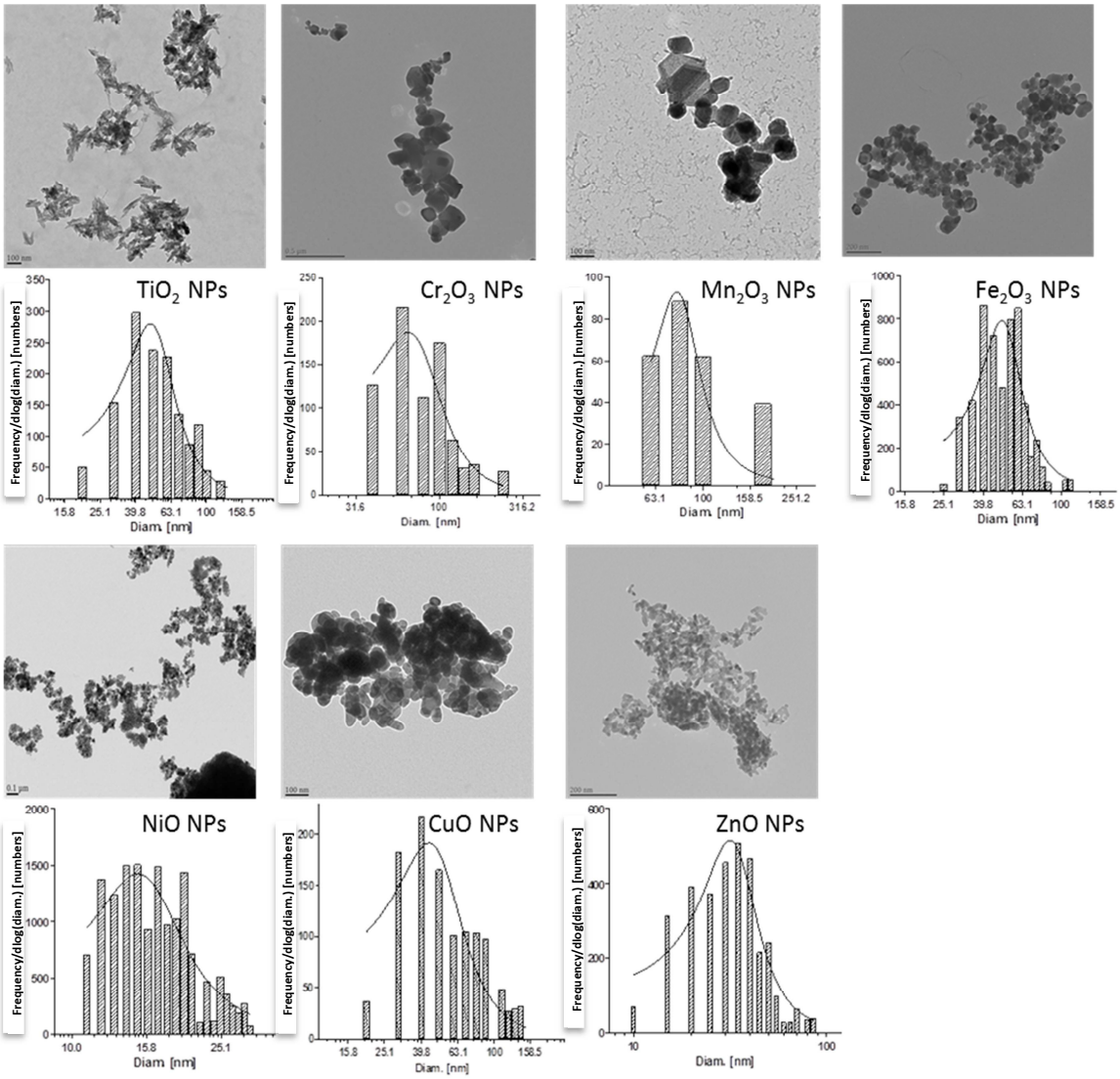

Figure A1. Morphology and size distribution of nanoparticles.

XPS analysis was not performed for all of the metal oxide NPs at pH = 4.5 since etching effects by acidity were observed, which skewed quantitative measurement. For example, when TiO_2 is subjected to the CC procedure maintaining pH at 4.5, an additional oxide peak at 529.0 eV forms, indicating chemical etching of the nanoparticles as observed in **Figure A2**.

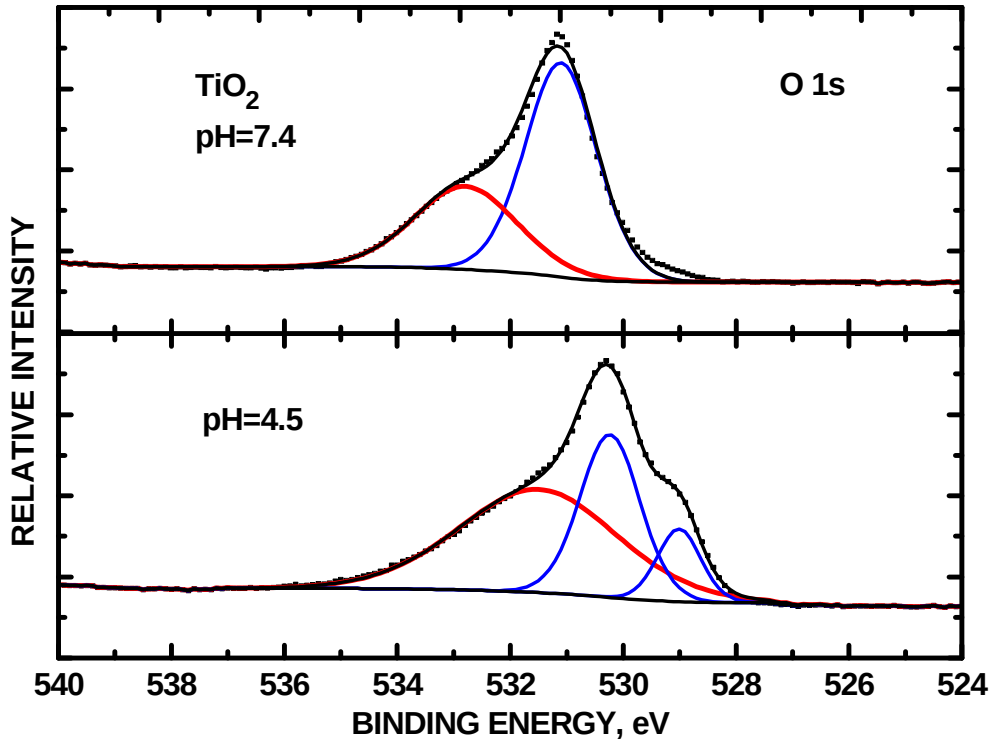

Figure A2. XPS stackplot of TiO_2 nanoparticulates after CC reactions at pH 7.4 (top) and 4.5 (bottom). The blue line denotes metal oxide oxygen while the red line denotes adsorbed non-metal oxide oxygen. At pH = 4.5, and additional oxide peak at 529.0 eV formed, indicative of chemical etching of the nanoparticles.

A1.5 Band-gap energy measurements

The term "band-gap" denotes the difference in energy between the top of the valence band and the bottom of the conduction band. Band gap can be spectroscopically determined from the transition between the strong absorption occurring at high-energy wavelengths and the weak absorption occurring at relatively low energy wavelengths. In the case of solids such as nanomaterials, which can be dispersed in a non-interfering liquid, the absorption edge can be measured using transmittance techniques. With the nanomaterials used in this study, 1-3 mg samples were dispersed in ~4 mL of H_2O or ethanol, and the transmittance spectra were measured in 1 cm cell in a Beckman DU 640B UV-vis spectrophotometer.

A1.6 Measurement of metal dissolution from transition metal oxide nanoparticles by ICP-MS and GFAA

Metal ion dissolution analysis was performed following the constant composition procedure of the metal oxides in aqueous solution. CC reactions for 24 hr periods at pH = 7.4 and pH = 4.5 were performed to ensure equilibrium conditions prior to analysis. Batch CC reactions for each metal oxide were performed using a Metrohm 702 SM Titrino apparatus equipped with autotitrator (Riverside, FL). Aliquots of the stored solutions were placed in polypropylene centrifuged tubes washed with 3% HNO_3 overnight, rinsed with Millipore water, and centrifuged at 20,000g for 5 min using a Thermo Scientific Sorvall Evolution RC superspeed centrifuge equipped with a SS34 rotor. Much of the oxide particles were recovered at the bottom of the tube. Then, 2 mL of the topmost liquid was pippeted into a Spectra/Por Biotech cellulose ester dialysis membrane with a molecular weight cut-off of 100-500 Daltons (Spectrum Laboratories; Rancho Dominguez, CA), and placed into 30-mL glass tubes filled with 25 mL of Millipore water. Laser light (633 nm wavelength) was propagated through the solutions to ensure that no solid particulates were present as revealed by an absence of light scattering due to the Tyndall effect. Tubes for each metal oxide were then placed on a shaker to mechanically agitate the solution during the 16 h dialysis. Following dialysis, samples were extracted from the 30-mL glass tubes (outside the dialysis bag) for analysis. It should be noted that during preparations for dialysis, all materials were handled with non-metallic tools, and Teflon-coated scissors, forceps, and glass tubes were rinsed overnight in a 3% HNO_3 solution prior to use. The samples were stored at 4°C until analyzed by graphite furnace atomic absorption spectroscopy (GFAA) and inductively coupled plasma mass spectroscopy (ICP-MS).

Dissolved metal elements, Ti^{4+}, Cr^{3+}, Mn^{3+}, Ni^{2+}, Cu^{2+}, and Zn^{2+} were detected using an Elan-DRCe ICP-MS (Perkin-Elmer) equipped with a cyclonic spray chamber, a Meinhard nebulizer, platinum cones, and a CETAC ASX-500/ADX-100 autosampler. The ICP-MS analysis conditions were as follows: RF power was 1,300 W, argon flow rates for the plasma and auxiliary gas were 15 and 1.2 L/min, respectively, and samples were delivered at 1.0 ml/min by a peristaltic pump. Internal standards were added continuously online. Dissolved Fe^{3+} was detected using a graphite furnace atomic absorption spectrometry (Perkin-Elmer Analyst 600 GFAA spectrometer) method. A single-element Fe hollow cathode lamp was used. The matrix modifier was $Mg(NO_3)_2$. The absorbance was detected at the wavelength 248.3 nm and slit setting of 0.2 nm.

To ensure good quality data, QA/QC procedures recommended by the EPA methods were followed. Instrument responses were calibrated with standard solutions using a range of concentrations. The detection limits were calculated at signal/noise ratio 3 to 5. The linear ranges of the calibration were determined and used for the quantitative analysis of the samples. Good linearity (R^2 = 0.99-to-1.00) was obtained. The detection limits for Ti^{4+}, Cr^{3+}, Mn^{3+}, Ni^{2+}, Cu^{2+}, and Zn^{2+} were 0.02, 0.05, 0.02, 0.04, 0.03, and 0.05 ppb, respectively. The detection limit for Fe^{3+} was 2.0 ppb. Laboratory reagent blanks were prepared and measured using the same procedures except absence of the samples. At least one blank was prepared and measured for each batch of up to 20 samples. One or more duplicate samples were analyzed for each type of sample, and the relative percent difference (RPD) was calculated to ensure good precision. RPDs ranged from 0 to 6%. Water reference standards (High-Purity Standards, Charleston, SC, USA) were analyzed for each batch of samples. Laboratory sample spikes were also performed for each type of

sample for ICP-MS and GFAA analyses to ensure acceptable accuracy. Spike recoveries ranged from 93 to 123%. During analysis, calibration checks with standard solutions were performed frequently (every 10 to 12 samples) to monitor the instrument performance.

Table A1. Temporal changes of pH in cell culture medium (A549) with and without nanoparticles. Nanoparticles were dispensed into cell culture medium. The pH was measured at 0, 6, 12, 18, and 24 hours. Values are averages of 5 sampling time points.

Conc. (μg/mL)	5	15	25	50	75	100
TiO_2	0.01 ± 0.12	0.01 ± 0.12	0.04 ± 0.11	0.10 ± 0.11	0.13 ± 0.10	0.16 ± 0.13
Cr_2O_3	0.03 ± 0.08	0.10 ± 0.06	0.13 ± 0.06	0.18 ± 0.05	0.23 ± 0.04	0.31 ± 0.03
Mn_2O_3	0.04 ± 0.04	0.06 ± 0.06	0.11 ± 0.05	0.16 ± 0.07	0.21 ± 0.06	0.21 ± 0.10
Fe_2O_3	0.02 ± 0.06	0.05 ± 0.10	0.08 ± 0.08	0.11 ± 0.07	0.15 ± 0.07	0.16 ± 0.11
NiO	0.01 ± 0.12	0.01 ± 0.12	0.04 ± 0.11	0.10 ± 0.11	0.13 ± 0.10	0.16 ± 0.13
CuO	0.03 ± 0.18	0.07 ± 0.17	0.15 ± 0.15	0.21 ± 0.14	0.24 ± 0.12	0.29 ± 0.14
ZnO	0.04 ± 0.03	0.01 ± 0.04	0.14 ± 0.02	0.18 ± 0.03	0.20 ± 0.02	0.23 ± 0.07

Table A2. The available particle surface binding site as indicated by hydroxyl-to-metal oxide XPS integrated peak area ratio from O 1s orbital (pH = 7.4).

Metal oxide	[adsorbed oxygen]	[metal oxide O]	[adsorbed oxygen / metal oxide O]
TiO_2	5354.5	9637.6	0.56
Cr_2O_3	12710.5	4101.5	3.10
Mn_2O_3	4381.9	6144.2	0.71
Fe_2O_3	4935.2	4671.6	1.06
NiO	6977.3	2997.0	2.33
CuO	7419.6	1117.8	6.64
ZnO	10551.1	1560.0	6.76

A2. Discussion of Band Gap Energy

The band-gap of each metal oxide NP was spectroscopically determined. No correlation between cytotoxicity rank and band-gap rank (**Figure A3A**) was evident. For the calculation of the conduction and valence band energies, E_c and E_v respectively (**Table**

A3), the electronegativity of the metal oxide NP in electron volts, χ_{oxide} (eV), was determined according to

$$\chi_{cation}(\mathrm{Pu}) = 0.274z - 0.15zr - 0.01r + 1 + \alpha \quad (3)$$

$$\chi_{cation}(\mathrm{eV}) = \frac{(\chi_{cation}\ (\mathrm{Pu}) + 0.206)}{0.336} \quad (4)$$

$$\chi_{oxide}(\mathrm{eV}) = 0.45\chi_{cation}(\mathrm{eV}) + 3.36 \quad (5)$$

where χ_{cation}(Pu) is the electronegativity of the cation in Pauling units, z is the formal charge of the cation, r is the ionic radius of the cation in units of Å, α is an empirical modifying term, and χ_{cation}(eV) is the electronegativity of the cation in units of eV [11]. With these data it was possible to calculate E_c and E_v as

$$E_c = -\chi_{oxide} + 0.5E_g + 0.059(\mathrm{PZC} - \mathrm{pH}) \quad (6)$$

$$E_v = E_c - E_g \quad (7)$$

where E_g is the experimentally determined band-gap of each metal oxide, PZC is the experimentally determined point-of-zero charge of each metal oxide at pH = 7.4. The results are graphically depicted in **Figure A3B**. The cytotoxicity rank, 1 through 7, is shown for the seven metal oxides with "1" denoting the least toxic and "7" denoting the most toxic. According to the "band-gap hypothesis" [12-14], when the material band-gap (of the metal oxide NPs) at which electron transfer occurs overlaps the energy levels of biological redox couples (which are typically in the range of –4.12 to –4.84 eV [15]), the permissive electron transfers may result in redox reactions that decrease antioxidant levels, increase levels of ROS, and/or increase levels of oxidized biological materials.

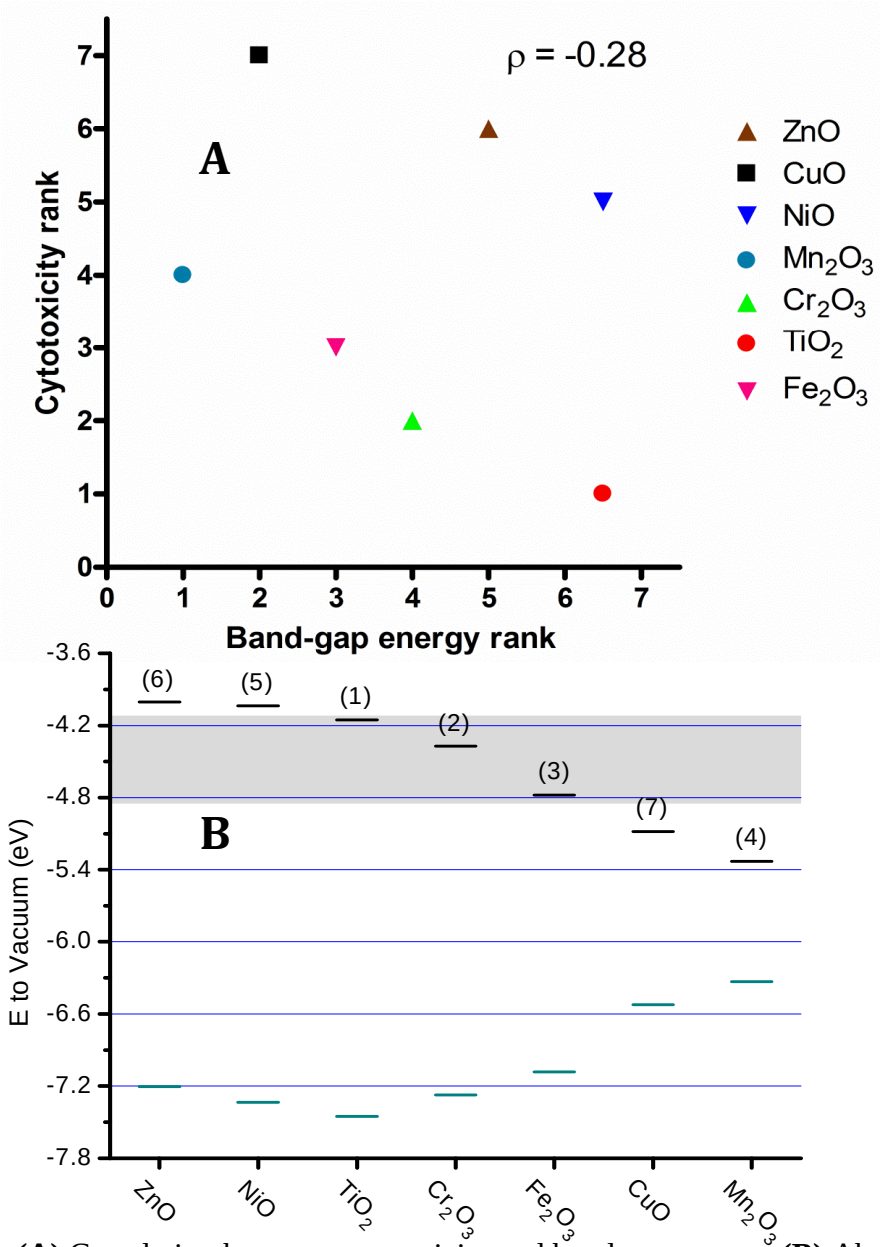

Figure A3. (A) Correlation between cytotoxicity and band gap energy; **(B)** Absolute positions of the conduction and valence bands for the materials relevant to this study. The grey area indicates the cellular redox potential (4.12–4.84 eV). The numbers in parentheses denote cytotoxicity rank.

Table A3. The spectroscopically determined band-gap, point of zero charge, PZC, position below the vacuum level of the valence and conduction bands, E_v and E_c respectively, cytotoxicity rank of each nanoparticle and the electronegativity of the metal oxide, χ_{oxide}.

Parameter	TiO_2	Cr_2O_3	Mn_2O_3	Fe_2O_3	NiO	CuO	ZnO
Band-gap (eV)	3.3	2.9	1.0	2.3	3.3	1.4	3.2
χ_{oxide} (eV)	5.8	5.9	5.7	5.9	5.7	5.9	5.7
PZC	6.8	8.0	8.9	8.2	8.4	8.6	8.6
E_c (eV)	-4.2	-4.4	-5.3	-4.8	-4.0	-5.1	-4.0
E_v (eV)	-7.5	-7.3	-6.3	-7.1	-7.3	-6.5	-7.2
Cytotoxicity rank	1	2	4	3	5	7	6

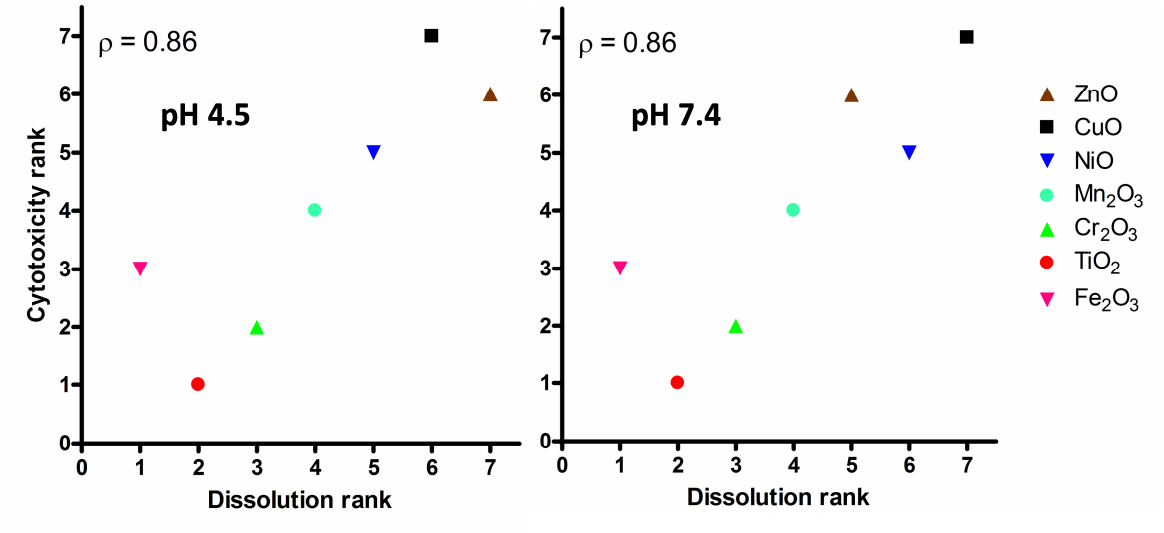

Figure A4. Correlation between cytotoxicity and metal dissolution from nanoparticles.

These actions result in elevated toxicity. The band-gaps of the three metal oxide NPs with the lowest ranked toxicity in this series (TiO_2, Cr_2O_3 and Fe_2O_3) overlapped with that region of the biological redox couples. The remaining metal oxide NPs, all of which are more toxic, lie outside of that region. Thus, our data suggests that NP band-gap does not play a role governing cytotoxicity.

REFERENCES

[1] S. Brunauer, P.H. Emmett, E. Teller, Adsorption of gases in multi-molecular layers, J. Amer. Chem. Soc. 60 (1938) 309-319.

[2] G.E. Brown, Jr., V. E. Henrich, W. H. Casey, D.L. Clark, C. Eggleston, A. Felmy, D. W. Goodman, M. Grätzel, G. Maciel, M. I. McCarthy, K. H. Nealson, D.A. Sverjensky, M.F. Toney, J.M. Zachara, Metal oxide surfaces and their interactions with aqueous solutions and microbial organisms, Chem. Rev. 99 (1999) 77-174.

[3] J. Park, J.R. Regalbuto, A Simple, Accurate Determination of Oxide PZC and the Strong Buffering Effect of Oxide Surfaces at Incipient Wetness, J. Colloid Interface Sci. 175 (1995) 239-252.

[4] M.R. McPhail, J.A. Sells, Z. He, C.C. Chusuei, Charging Nanowalls: Adjusting the Carbon Nanotube Isoelectric Point via Surface Chemical Functionalization, J. Phys. Chem. C 113 (2009) 14102-14109.

[5] C.C. Chusuei, D.W. Goodman, D. W. X-ray photoelectron spectroscopy, in: R.A. Meyers (Ed.), Encyclopedia of Physical Science and Technology, 3rd ed., Academic Press New York, 2002; Vol. 17, pp 921-938.

[6] T. L. Barr, Modern ESCA. CRC Press, Boca Raton, 1994; Vol.; Chapter 9, p 359.

[7] T. L. Barr, S. Seal, Nature of the use of adventitious carbon as a binding energy standard, J. Vac. Sci. Technol. A 13 (1995) 1239-1246.

[8] D.A. Shirley, High-resolution X-ray photoemission spectrum of the valence bands of gold, Phys. Rev. B 12 (1972) 4709-4714.

[9] C.C. Chusuei, D. W. Goodman, M.J. Van Stipdonk, D.R. Justes, K.H. Loh, E.A. Schweikert, Solid-liquid adsorption of calcium phosphate on TiO_2, Langmuir 15 (1999) 7355-7360.

[10] M.G. Nooney, A. Campbell, T.S. Murrell, X.-F. Lin, L.R. Hossner, C.C. Chusuei, D.W. Goodman, Nucleation and growth of phosphate on metal oxide thin films, Langmuir 15 (1998) 2750-2755.

[11] J. Portier, G. Campet, A. Poquet, C. Marcel, M.A. Subramanian, Degenerate Semiconductors in the Light of Electro-negativity and Chemical Hardness, Int. J. Inorg. Mater. 3 (2001) 1039-1043.

[12] E. Burello, A.P. Worth, QSAR modeling of nanomaterials, Wiley Interdiscip. Rev.: Nanomed. Nanobiotechnol. 3 (2011) 298-306.

[13] H. Zhang, Z. Ji, T. Xia, H. Meng, C. Low-Kam, R. Liu, S. Pokhrel, S. Lin, S., X. Wang, Y.-P. Liao, M. Wang, L. Li, R. Rallo, R. Damoiseaux, D. Telesca, L. Mädler, Y. Cohen, J. I. Zink, A. E. Nel, Use of metal oxide nanoparticle band gap to develop a predictive paradigm for oxidative stress and acute pulmonary inflammation. ACS Nano 6 (2012) 4349-4368.

[14] E. Burello, A.P. Worth, A theoretical framework for predicting the oxidative stress potential of oxide nanoparticles, *Nanotoxicol.* 5 (2011) 298-306.

[15] G.S. Plumlee, S.A. Morman, T.L. Ziegler, The toxicological geochemistry of earth materials: an overview of processes and the interdisciplinary methods used to understand them, Rev. Mineral Geochem. 64 (2006) 5-57.